# Electrical properties and aging behavior of nickel manganite thin films co-doped with Cu and Zn annealed at low temperature

**Duc Thang Le** ( ducthang36@skku.edu )
Gachon University
**Heongkyu Ju**
Gachon University

**Research Article**

**Keywords:** Liquid flow deposition, Thin films, Spinels, Stability, Zinc, Nickel manganites

**Posted Date:** April 3rd, 2020

**DOI:** https://doi.org/10.21203/rs.3.rs-20791/v1

# Abstract

Nickel-manganite-based thin films with a negative temperature coefficient of resistance (NTCR) characteristic were prepared from (Ni 0.2 Mn 2.8– x Cu x )Cl 2 (0.010£ x £0.040) solutions using the liquid flow deposition (LFD) method. The influence of Cu on the electrical properties of the films annealed at 400 °C was investigated. Adding Cu ( x = 0.025) was found to quite effectively lower the electrical resistivity ( ρ ) of the films to 200 W cm, whereas their sensitivity behavior was significantly degraded. Interestingly, the absolute temperature coefficient of resistance ( TCR ) of the films was enhanced by further adding 0.01 mol Zn along with Cu, without a remarkable increase in ρ . TCR = 2.98% K – 1 and ρ = 880 W cm at room temperature were attained for the Zn-containing specimen with 0.020 mol Cu doping. Moreover, the films with (Zn,Cu) co-doped compositions showed a much higher electrical stability than the Zn-free films.


# 1. Introduction

Nickel manganite oxide ceramics with a negative temperature coefficient of resistance (NTCR) characteristic have been attracting substantial attention for several decades [1, 2]. These materials have been used for infrared sensing applications due to their high temperature sensitivity, fast response, cost-effectiveness, adaptable size, and practical convenience [3, 4]. Generally, the nickel manganite system exhibits a spinel-type structure with the general formula $AB_2O_4$ (A: tetrahedral and B: octahedral sites), and its electrical conductivity is typically described in terms of the electron hopping conduction between $Mn^{3+}$ and $Mn^{4+}$ states at octahedral sites, induced by lattice vibrations [3, 5, 6].

In practice, some applications such as microbolometers require NTCR materials with low electrical resistivity (ρ), large temperature coefficient of resistance (TCR), and sufficient stability. Modifying the composition of nickel manganite compounds with appropriate transition metal ions (suitable for tetrahedral sites occupation) has been found to allow $Ni^{2+}$ to occupy octahedral sites, thus improving the electrical conductivity [7]. Among various elements, Cu has been reported as the most effective ion for lowering the resistivity; unfortunately, Cu doping also degrades the electrical stability [7–9]. Chen et al. reported that Cu doping decreased the resistivity of $Ni_{0.5}Mn_{2.5}O_4$ ceramics as low as 70 Ω cm, but simultaneously raised the resistivity drift up to 14.9% [10]. In this regard, adding Zn is known to effectively stabilize the spinel structure against the oxidation reaction when partially replacing Mn in nickel manganite compounds [11, 12]. Ma and co-workers investigated the effects of Zn doping on the aging characteristic of $Ni_{0.6}Cu_{0.5}Zn_xMn_{1.9-x}O_4$ ceramics, and they demonstrated that the resistivity drift significantly decreased from 10.2% for the undoped samples to 0.02% for the samples with Zn doping of x = 0.75 [13]. The authors also emphasized that the thermal constant (B) of the ceramics was improved by Zn doping. Thus, Cu and Zn greatly benefit the electrical conductivity and stability, and hence, the combined effects of these ions on nickel manganite spinel materials are worth investigating.

The electrical and physical properties of NTCR nickel manganite have been widely studied, but mostly in bulk and thick-film forms. Unfortunately, poor stability and reproducibility have been reported for bulk

ceramics [14], and the thick films show low sinterability [15]. Furthermore, the bulks and thick films commonly require high sintering temperatures [5, 7–12, 14, 15]. Dense polycrystalline thin films that can be synthesized at relatively lower temperatures are considered to overcome these shortcomings. Thin films have also been confirmed to increase output responses and decrease operating voltages [3, 5]. Meanwhile, the current trend in electronics technology is to reduce the dimensions of the electronic components; therefore, fabricating passive components using the thin-film technique is an emerging solution.

Thin films are prepared using various methods, among which chemical solution processes have attracted considerable attention because of their low cost, simplicity, and large area coverage. Among them, liquid flow deposition (LFD), which typically provides the advantages of low processing temperatures and environmental friendliness, offers great potential for synthesizing crystallized nickel-manganite-based thin films [16]. Particularly, by exploiting the $Mn^{2+} \rightarrow Mn^{3+}$ oxidation, high-quality NTCR $(Co,Ni,Mn)_3O_4$ thin films have been successfully fabricated via the LFD route, as described in our previous work [17]. The cubic spinel structure forms at an annealing temperature of 400 °C and yields highly conductive films. In terms of the conductivity mechanism, many studies have modified the composition of nickel-manganite thin films with various substituting/doping cations; however, most authors focused only on synthesis temperatures above 500 °C [4, 5], whereas few studies have prepared thin films at low temperatures thus far. In the present study, we demonstrate the effect of Zn and Cu co-doping on the phase, morphology, electrical properties, and aging behavior for LFD $(Ni,Mn)_3O_4$-based thin films annealed at 400 °C.

## 2. Experimental Procedure

## 2.1. Precursor solution preparation

$MnCl_2{\cdot}4H_2O$, $NiCl_2{\cdot}6H_2O$, $CuCl_2{\cdot}2H_2O$, and $ZnCl_2{\cdot}4H_2O$ supplied by Sigma-Aldrich were used as raw materials for preparing reaction solutions with the following compositions:

1. $(Ni_{0.2}Mn_{2.8-x}Cu_x)Cl_2$ with $x$=0.000, 0.010, 0.015, 0.020, 0.025, 0.030, 0.035, and 0.040
2. $(Ni_{0.2}Zn_{0.1}Mn_{2.7-x}Cu_x)Cl_2$ with $x$=0.000, 0.010, 0.015, 0.020, 0.025, and 0.030.

Deionized (DI) water was used to dissolve these compounds to form 50 mM solutions. As the solutions were continuously stirred, an appropriate amount of $NH_4Cl$ was added and mixed. After 1 h of stirring, the resulting solutions were used as precursor solutions to deposit thin films.

## 2.2. Thin-film deposition

The experimental process of thin-film deposition via LFD was described in detail in our earlier report [19]. In the present work, to prevent precipitation, the pH was adjusted in a range of 6.65–6.85 by adding ammonia ($NH_3.H_2O$). The reactant and oxidizing solutions ($H_2O_2$, 5 mM) simultaneously flowed into the deposition chamber at rates of 400 and 100 mL/h, respectively, where an upside-down $Si/SiN_x$ wafer (2.5

× 2.5 $cm^2$) was already located. The substrate temperature was maintained constant at 60 °C throughout the deposition. The growing time was set to 8 h for each sample. After deposition, the films were washed with DI water and then dried at 100 °C for 2 h in an oven. Finally, all the specimens were annealed at 400 °C for 5 h in air (with a heating rate of 5 °C/min) and then naturally cooled.

## 2.3. Characterizations

Atomic force microscopy (AFM, Neos, Bruker, Germany) and field-emission scanning electron microscopy (FE–SEM, JEOL, Japan) were employed to examine the surface morphology of the films. X-ray diffraction (XRD, Rigaku, Japan) was conducted to determine the crystal structure. The oxidation states of copper were examined by an X-ray photoelectron spectroscopy (XPS) system (VG ESCA 3000). The sheet resistance–temperature dependence (R–T) of the films was measured in a temperature range from 22 °C to 95 °C using a four-point probe system (DSF system, Doosung, Korea). From R–T data, the TCR was calculated by a universal equation given in ref [3]. To test the stability, the films were aged in an oven at 150 °C (in air), and the room-temperature (RT) sheet resistance was measured at various points during aging, up to 500 h. The aging coefficient was defined as $\Delta R/R_o = (R–R_o)/R_o$ (%), in which $R_o$ and R are the resistance at RT before and after aging, respectively [18].

# 3. Results And Discussion

## 3.1. Microstructure and crystal structure analyses

For the Cu-doped film series, deposited at pH = 6.85, a compact surface was achieved for the as-grown films with a small amount of Cu ($x \leq 0.025$). Figure 1a–c shows topographical AFM images of the surface of samples with x = 0.000, 0.015, and 0.025, respectively. The films reveal a uniform morphology without any cracks; no significant morphological differences were found among these films, except for an increase in the grain size, as listed in Table 1. However, the FE–SEM observations in Fig. 2a–c clearly display the degradation in the surface quality of the thin films with high Cu levels ($x \geq 0.030$). As x reaches 0.035, the film shows many pores on the surface as clearly seen in Fig. 2b. When x further increases to 0.040 (Fig. 2c), the porosity becomes much higher, resulting in a poorer microstructure and a decrease in thickness.

Table 1

Grain size, roughness, and thickness of films

| x | Zn-free | | | Zn-added | | |
|---|---|---|---|---|---|---|
| | Mean grain size (nm) | Roughness (nm) | Thickness (nm) | Mean grain size (nm) | Roughness (nm) | Thickness (nm) |
| 0.000 | 50 | 17.7 | 420 | 4 | – | 300 |
| 0.015 | 60 | 22.5 | 450 | 7 | – | 280 |
| 0.025 | 70 | 23.1 | 400 | 10 | 4.1 | 280 |
| 0.030 | 70 | 31.8 | 400 | 13 | 6.7 | 270 |
| Annealing temperature: 400 °C | | | | | | |
| The average grain size was evaluated from surface images acquired by FE–SEM and AFM and using ImageJ software. | | | | | | |
| The roughness was calculated using an AFM scanning probe image processor (SPIP–4.8.2) software. | | | | | | |
| The thickness was evaluated from cross-sectional FE–SEM images. | | | | | | |

The (Zn,Cu) co-doped $(Ni,Mn)_3O_4$ thin films were prepared from nickel manganese chloride solutions by simultaneously adding 0.01 mol $ZnCl_2$ and x (0.000–0.030) mol $CuCl_2$ under the same conditions as for the Cu-doped-only films, except that the solution pH was adjusted to decrease from 6.85 to 6.65. The AFM photographs of as-grown Zn-added thin films with x = 0.000, 0.015, and 0.025 are also shown in Fig. 1. Comparing the AFM images of specimens with and without Zn indicates that both, the Zn-free and Zn-added films, have grains with a spherical morphology; however, adding Zn results in a smooth surface with much finer grains (Table 1). On the other hand, the thickness of each film series does not substantially change, varying within 400–450 nm for the Cu-doped and 270–300 nm for the (Zn,Cu) co-doped films (Fig. 2d and Table 1).

The crystal structure of the annealed Zn-free and Zn-added films was analyzed by XRD, and the results are shown in Fig. 3. As presented in Fig. 3a and b, all films are well-crystallized after heat treatment in air at 400 °C. The high crystallization of the LFD nickel manganite-based thin films after annealing at a moderate temperature has been discussed elsewhere [16, 17]. A tetragonal spinel structure is revealed for films without Cu (x = 0.000), regardless of the presence of Zn in their compositions. However, the (221) tetragonal spinel peak for Zn-added film shifts to a slightly higher angle, as observed in Fig. 3c, which can be attributed to the replacement of $Mn^{2+}$ ions with $Zn^{2+}$ ions at the tetrahedral sites of the spinel. As the ionic radius of the $Zn^{2+}$ cation (0.58 Å) is smaller than that of the $Mn^{2+}$ cation (0.66 Å) [13], this replacement decreases the lattice parameter in the spinel phase, thus shifting the corresponding peak. On the other hand, cubic symmetry (Fd–3 m space group) appears when $x \geq 0.010$ for both systems (referring to JCPDS card No. 84–0542), without any secondary phases. This finding demonstrates that Cu, rather

than Zn, induces the transformation from the tetragonal to the cubic spinel structure in the present $(Ni,Mn)_3O_4$-based specimens. The (311) peak shows the highest intensity for all cubic spinel patterns, clearly indicating the preferential orientation of the films. The XRD pattern characteristics and changes in the intensity are very similar as x increases in both systems, even though the adding Zn has been reported to improve the crystallinity in the case of spin-sprayed nickel manganite thin films [19]. Moreover, the peak intensity uniformly increases with increasing x, demonstrating that Cu increases the crystallinity.

# 3.2. Electrical properties

Figure 4a depicts the (ρ)–temperature (T) curve in the testing temperature range T = 295–368 K (22–95 °C) for the annealed Zn-free samples. This figure clearly shows that the resistivity decreases with increasing testing temperature, demonstrating a typical NTCR feature for the films. On the other hand, the lnR/T and reciprocal of the absolute temperature (1000/T) in Fig. 4b clearly present a nearly linear relationship over the measured temperature range. This linear dependence should be attributed to the electron hopping conduction mechanism, for which the R–T relationship is commonly described by the well-known expression: $R = CTexp(Ea/k_BT)$, where C is a constant, and T, $E_a$, and $k_B$ are the absolute temperature, activation energy for electrical conduction, and Boltzmann constant, respectively [3, 5]. Results similar to those in Fig. 4 were confirmed for all the annealed Zn-added films.

Figure 5a presents the RT resistivity (ρ) of films examined as a function of the Cu doping level, x. For the Zn-added system, the resistivity rapidly decreases to a minimum value of 880 Ω cm when x is increased from 0 to 0.02, and then increases slightly with further increases in x. In a similar manner, the Zn-free films also show a decrease in ρ with $x \leq 0.025$ and a tendency to increase with $x \geq 0.03$. The lowest ρ value of 200 Ω is achieved when x = 0.025. Compared with the Zn-free films at x = 0.000, an increase in resistivity from 6,300 Ω cm to 9,210 Ω cm is observed for the Zn-added films. Although the resistivity does not change much, this result clearly indicates that Zn doping deteriorates the conductivity. The Hall carrier concentration and mobility for the Zn-free films, as presented in Table 2, show that the carrier concentration systematically increases, whereas the carrier mobility decreases with Cu in the films. Therefore, the tendency of ρ to decrease in Fig. 5a should be attributed to the carrier concentration rather than the carrier mobility. On the other hand, the mobility of the charge carriers decreases in the Cu-rich compositions, possibly because the ionized Cu atoms act as scattering centers at a high carrier concentration, thereby decreasing the carrier mobility. Consequently, we suggest that the increased electrical conductivity of the Cu-doped films is mainly due to changes in the carrier concentration, caused by the combined effects of the composition and crystal structure.

Table 2
Carrier concentration and carrier mobility of Zn-free films

| x | Carrier concentration ($cm^{-3}$) | Carrier mobility ($cm^2/V{\cdot}s$) |
|---|---|---|
| 0.000 | $4{,}44 \times 10^{13}$ | 29.0 |
| 0.010 | $8.57 \times 10^{13}$ | 25.4 |
| 0.015 | $1.37 \times 10^{14}$ | 25.5 |
| 0.020 | $2.87 \times 10^{14}$ | 24.7 |
| 0.025 | $7.35 \times 10^{14}$ | 20.4 |
| 0.030 | $8.79 \times 10^{14}$ | 16.0 |

In Cu-doped nickel manganite spinels, monovalent copper ($Cu^{+}$) is known to reside at the tetrahedral sites, while bivalent copper ($Cu^{2+}$) occupies both, the octahedral and tetrahedral sites of the spinel [20, 21]. The presence of $Cu^{+}$ increases the amount of cations in the tetrahedral sublattices, which in turn displaces some $Ni^{2+}$ cations from tetrahedral to octahedral sites. This process produces $Mn^{4+}$ at octahedral sites to maintain the electrical neutrality, consequently increasing the $Mn^{4+}$concentration. As more $Mn^{4+}$ ions are generated, a larger number of sites are available for electron hopping, which could be the possible reason for the improved carrier concentration in Table 2, which contributes to the electrical conductivity of the present two types of films.

Many researchers have suggested that $Zn^{2+}$ is located only at tetrahedral sites [10, 11, 22]. Thus, it is reasonable to infer that the Cu cations are expelled from tetrahedral sites and move into octahedral sites in the (Zn,Cu) co-doped compositions. This process changes $Cu^{+}$ into $Cu^{2+}$; consequently, the $Cu^{+}$ cation concentration at the tetrahedral sites decreases. Moreover, as $Cu^{+}$ changes into $Cu^{2+}$, $Mn^{4+}$ transforms into $Mn^{3+}$ to maintain the electrical neutrality of the lattice [13], which eventually increases the electrical resistivity of the Zn-added films, as shown in Fig. 5a. The much finer grain size with added Zn, as shown in Fig. 1, should be also taken into account to better explain the differences between the conductivities of these two film systems.

Cu doping is found to decrease the absolute RT TCR from 3.21 to 2.38% $K^{-1}$ for the Zn-free system, as depicted in Fig. 5b. Clearly, Cu doping provides a significant decrease in the resistivity, but degrades the film sensitivity. A drop in TCR with Cu doping was also reported by Cho et al. [9] for spin-sprayed nickel manganite thin films, but the possible reasons for this behavior are still under investigation. On the other hand, the presence of Zn in the compositions is found to improve the TCR, which varies in the range of 2.82 to 3.54% $K^{-1}$ for the (Zn,Cu) co-doped system. The measured TCR values are even better than the results obtained for sputtered Ni–Co–Mn–O films, where the absolute TCR of $\geq$ 3% $K^{-1}$ was only achieved when the resistivity was higher than 1,000 Ω cm [23, 24]. Notably, in the present work, co-doping

0.01 mol Zn along with Cu remarkably enhances the TCR, whereas it only moderately deteriorates the conductivity. For instance, a high TCR of 3.02% $K^{-1}$ and a resistivity as low as 880 Ω cm are simultaneously achieved for the Zn-added film with x = 0.020. These excellent electrical features are interesting for infrared sensing applications such as microbolometers.

# 3.3. Electrical stability

Figure 6a shows the resistance drift ($\Delta R/R_o$) for films with and without added Zn after aging at 150 °C in air for 500 h. As expected, a high resistance drift of up to 10.5% is revealed for the Zn-free samples, which is much larger than that for the (Zn,Cu) co-doped specimens, which was below 6.1%. This result confirmed the strong effect of Zn on the electrical stability. The most conductive Zn-added film (x = 0.020) possesses $\Delta R/R_o$ = 5.4%, whereas the lowest $\Delta R/R_o$ = 5.2% is attained for one film where x = 0.025. Figure 6b shows the detailed aging history of the x = 0.020 Zn-containing film, which demonstrates that the film undergoes a sudden increase in resistance during the first 82 h of aging. Subsequently, the increasing tendency of the resistance tends to slow down and reaches a nearly saturated state after 215 h, with a resistance drift of 5.2%. Up to 500 h of aging, the overall resistance drift is 5.4%.

The mechanism underlying the drift in the resistance of Cu-doped nickel manganite spinels has been interpreted as the $Cu^+$ ions at tetrahedral sites easily oxidizing to $Cu^{2+}$ under aging conditions (at temperatures ≤300 °C in air), which causes Cu ions to migrate from the tetrahedral to the octahedral sites [25]. This finding implies that the resistance drift is associated with a decrease in Cu cations at tetrahedral sites. To confirm this finding, the oxidation states of Cu before and after aging were verified by XPS analysis in $Cu2p_{3/2}$ region. The XPS experiments were performed on the most conductive specimens for each system. The order of binding energies in the $Cu2p_{3/2}$ region is $Cu^+$ (Te) < $Cu^{2+}$ (Oc) < $Cu^{2+}$ (Te) [26, 27], as presented in Fig. 7. The $Cu2p_{3/2}$ XPS characteristics are listed in detail in Table 3. Figure 7a1–2 distinctly shows that for the Zn-free film with x = 0.025, aging decreases the $Cu^+$ ion concentration at the tetrahedral sites and increases the $Cu^{2+}$ ion concentration at the octahedral sites (see also Table 3). In contrast, in the case of the (Zn,Cu) co-doped film with x = 0.020, neither the $Cu^+$ nor $Cu^{2+}$ ions change much after 500 h of aging, as can be observed in Fig. 7b1–2 and Table 3. These smaller variations in the amounts of $Cu^+$ and $Cu^{2+}$ ions can be attributed to the fact that $Zn^{2+}$ ions almost exclusively occupy the tetrahedral sites, and thus, the Cu ions with a valence of only 2 + predominantly reside at the octahedral sites. Therefore, the migration of Cu ions from the tetrahedral to the octahedral sites would be less pronounced, which possibly explains the higher stability of these films. In addition, the smooth surfaces in these film surfaces may reduce the adsorption of oxygen, which hinders the oxidation of $Cu^+$ ions. Notably, the aging performance of the (Zn,Cu) co-doped films in this study, which attain a resistance drift of 5.2–6.1%, is better than that of the undoped nickel manganite films prepared by spin-spraying and annealed at 400 °C in Ar, which exhibited a resistance drift of 6.5% for the same aging time [28]. However, this drift is still higher than those of the Mn–Co–Ni–O thin films annealed at 650–800 °C in air (1.7–5.2%) [29].

Table 3
Characteristics of the XPS $Cu2p_{3/2}$ spectra of Zn-free (x = 0.025) and Zn-added (x = 0.020) films

| Samples | Binding energy (eV) | | | Peak intensity (area %) | | |
|---|---|---|---|---|---|---|
| | $Cu^{+}$ (Te) | $Cu^{2+}$ (Oc) | $Cu^{2+}$ (Te) | $Cu^{+}$ (Te) | $Cu^{2+}$ (Oc) | $Cu^{2+}$ (Te) |
| Zn-free* | 931.1 | 933.0 | 943.4 | 37.1 | 34.0 | 28.9 |
| Zn-free# | 931.1 | 934.0 | 934.3 | 20.8 | 42.5 | 36.7 |
| Zn-added* | 930.9 | 933.9 | 934.5 | 24.4 | 32.2 | 43.2 |
| Zn-added# | 931.0 | 933.8 | 934.6 | 20.2 | 34.1 | 45.7 |
| * Before aging. | | | | | | |
| # After aging at 150 °C in air for 500 h. | | | | | | |
| Te and Oc refer to tetrahedral and octahedral sites, respectively. | | | | | | |

# 4. Conclusion

Thin films were prepared from an aqueous solution $(Ni_{0.2}Mn_{2.8-x}Cu_x)Cl_2$ (x = 0.010–0.040) via LFD. Films with smooth surfaces were achieved when $x \leq 0.030$, and a heat treatment at 400 °C in air enabled the crystallization of films with a cubic spinel structure. Cu doping quite effectively reduced the electrical resistivity of nickel manganite films (ρ) from 6,300 to 200 Ω cm, but also significantly decreased the TCR from 3.21 to 2.38%$K^{-1}$. Interestingly, the TCR was improved by adding 0.01 mol Zn along with Cu, accompanied by only a moderate increase in ρ. The Zn-added specimen with 0.020 mol Cu doping exhibited TCR = 3.02% $K^{-1}$ and ρ = 880 Ω cm at RT, offering potential for infrared sensing applications. Moreover, adding Zn increased the electrical stability, as the resistance drift reached 5.2% after aging at 150 °C in air for 500 h.

# Declarations

Acknowledgements
This research was financially supported by the Basic Science Research Program through the National Research Foundation of Korea (NRF) funded by the Ministry of Education (NRF–2017R1D1A1B03033987).

# References

1. Hou, Z. M. Huang, Y. Q. Gao, Y. J. Ge, J. Wu, and J. H. Chu, Characterization of $Mn_{1.56}Co_{0.96}Ni_{0.48}O_4$ films for infrared detection, Appl. Phys. Lett. 2008, **92**: 202115.
2. Ravi Kumar, S. K. Arora, I. V. Shvets, N. E. Rajeevan, P. P. Pradyumnan, K. Shukla, Structural and transport properties of Bi–substituted $Co_2MnO_4$, J. Appl. Phys 2009, **105**: 07D910
3. Feteira, Negative Temperature Coefficient Resistance (NTCR) Ceramic Thermistors: An Industrial Perspective, J. Am. Ceram. Soc. 2009, **92**: 967–983.
4. Schulze, J. Li, E. C. Dickey, and S. Trolier–McKinstry, Synthesis, Phase Characterization, and Properties of Chemical Solution–Deposited Nickel Manganite Thermistor Thin Films, J. Am. Ceram. Soc. 2009, **92**: 738–44.
5. Hou, Z. Huang, Y. Gao, Y. Ge, J. Wu, J. Chu, Characterization of $Mn_{1.56}Co_{0.96}Ni_{0.48}O_4$ films for infrared detection, Appl. Phys. Lett. 2008, **92**: 202115.
6. Sachse HF, Semiconducting Temperature Sensors and their Applications. New York: Wiley; 1975.
7. Metz, Electrical properties of N.T.C. thermistors made of manganite ceramics of general spinel structure: $Mn_{3-x-x'}M_xN_xO_4$ ($0 \leq x + x' \leq 1$; M and N being Ni, Co or Cu). Aging phenomenon study. J. Mater. Sci. 2000, **35**: 4705–4711.
8. N. Jadhav, Vijaya Puri, Influence of copper substitution on structural, electrical and dielectric properties of $Ni_{(1-x)}Cu_xMn_2O_4$ ($0 \leq x \leq 1$) ceramics, J. Alloys Compd. 2010, **507**: 151–156.
9. J. Jeon, Y.H. Jeong, J.S. Yun, W.I. Park, J.H. Paik, Y.W. Hong, E.S. Kim, J.H. Cho, Electrical properties of copper–nickel manganite thin films prepared by metal–organic decomposition, Ceram. Int. 2017, **43**: 9291–9295.
10. H. Zhao, B.Y. Wang, P.H. Yang, L. Winnubst, C.S. Chen, Effects of Cu and Zn co–doping on the electrical properties of $Ni_{0.5}Mn_{2.5}O_4$ NTC ceramics J. Eur. Ceram. Soc. 2008, **28**: 35–40.
11. Chanel, S. Guillemet–Fritsch, J. Sarrias, A. Rousset, Microstructure and electrical properties of Ni–Zn manganite ceramics. Int. J. Inorg. Mater. 2000, **2**: 241–247.
12. S. Aleksic, M.V. Nikolic, M.D. Lukovic, N. Nikolic, B.M. Radojcic, M. Radovanovic, Z. Djuric, M. Mitric, P.M. Nikolic, Preparation and characterization of Cu and Zn modified nickel manganite NTC powders and thick film thermistors, Mater. Sci. Eng. B 2013, **178**: 202–210.
13. Ma, Y. Liu, Y. Lu, H. Gao, H. Qian, J. Ding, Effect of Zn substitution on the phase, microstructure and electrical properties of $Ni_{0.6}Cu_{0.5}Zn_xMn_{1.9-x}O_4$ ($0 \leq x \leq 1$) NTC ceramics, Mater. Sci. Eng., B 2014, **188**: 66–71.
14. Jagtap, S. Rane, S. Gosavi, D. Amalnerkar, Low temperature synthesis and characterization of NTC powder and its 'lead free' thick film thermistors, Microelectron. Eng. 2010, **87**: 104–107.
15. Ryu, K.Y. Kim, J.J. Choi, B.D. Hahn, W.H. Yoon, B.K. Lee, et al. Flexible dielectric $Bi_{1.5}Zn_{1.0}Nb_{1.5}O_7$ thin films on a Cu–polyimide foil, J. Am. Ceram. Soc. 2009, **92**: 524–527.
16. T Le, C.J. Jeon, K.W. Lee, Y.H. Jeong, J.S. Yun, D.H. Yoon, J.H. Cho, Liquid flow deposited spinel $(Ni,Mn)_3O_4$ thin films for microbolometer applications, Appl. Surf. Sci. 2015, **330**: 366–373.

17. T Le, C.J. Jeon, K.W. Lee, Y.H. Jeong, J.S. Yun, D.H. Yoon, J.H. Cho, Characterization of ternary $(Ni,Co,Mn)_3O_4$ thin films for microbolometer applications, J. Alloys Compd. 2015, **650**: 415–420.
18. A. Kukuruznyak, J. G. Moyer, and F. S. Ohuchi, “Improved Aging Characteristics of NTC Thermistor Thin Films Fabricated by a Hybrid SolGel–MOD Process,” J. Am. Ceram. Soc. 2006, **89**: 189–92.
19. W. Ko, J. Li, N.J. Podraza, E.C. Dickey, S.T. McKinstry, Spin Spray–Deposited Nickel Manganite Thermistor Films for Microbolometer Applications, J. Am. Ceram. Soc. 2011, **94**: 516–523.
20. Lenglet, A D’Huysser, J. Kasperek, J.P. Bonnelle, J. Durr, Characterization of the oxidation states of copper and manganese in some manganites by the analysis of the XPS spectrum, X emission, and X absorption thresholds, Mater. Res. Bull. 1985, **20**: 745–757.
21. Elbadraoui, J.L. Baudour, F. Bouree, B. Gillot, S. Fritsch, A. Rousset, Cation distribution and mechanism of electrical conduction in nickel–copper manganite spinels, Solid State Ionics. 1997, **93**: 219–225.
22. Ajmal, A. Maqsood, Influence of zinc substitution on structural and electrical properties of $Ni_{1-x}Zn_xFe_2O_4$ ferrites, Mater. Sci. Eng. B 2007, **139**: 164–170.
23. Baliga, A. L. Jain, and W. Zachofsky, Sputter Deposition and Characterization of Ni–Mn–O and Ni–Co–Mn–O Spinels on Polymide and Glass Substrates, Appl. Phys. A 1990, **50**: 473–477.
24. Dannenberg, S. Baliga, R. J. Gambino, A. H. King, Resistivity, thermopower and the correlation to infrared active vibrations of $Mn_{1.56}Co_{0.96}Ni_{0.48}O_4$ spinel films sputtered in an oxygen partial pressure series, J. Appl. Phys. 1999, **86**: 514–523.
25. Gillot, S. Buguet, E. Kester, C. Baubet, P. Tailhades, Cation valencies and distribution in the spinels $Co_xCu_yMn_zFe_uO_{4+\delta}$ ($\delta \geq 0$) thin films studied by X–ray photoelectron spectroscopy, Thin Solid Films 1999, **357**: 223–231.
26. Low Temperature Crystallization of Metastable Nickel Manganite Spinel Thin Films, J. Am. Ceram. Soc., 2012, **95**: 2562–2567.
27. Topfer, A. Feltz, Preparation and electrical properties of the spinel series $Cu_zNiMn_{2-z}O_4$, Solid State Ionics 1993, **59**: 249–256.
28. Lenglet, A. d'Huysser, J. Kasperek, J.P. Bonnelle, J. Dürr, Characterization of the oxidation states of copper and manganese in some manganites by the analysis of the XPS spectrum, X emission, and X absorption thresholds, Mater. Res. Bull. 1985, **20**: 745–757.
29. He, Z.Y. Ling, Y.T. Huang, Y.S. Liu, Effects of annealing temperature on microstructure and electrical properties of Mn–Co–Ni–O thin films, Materials Letters 2011 **65**: 1632–1635.

# Figures

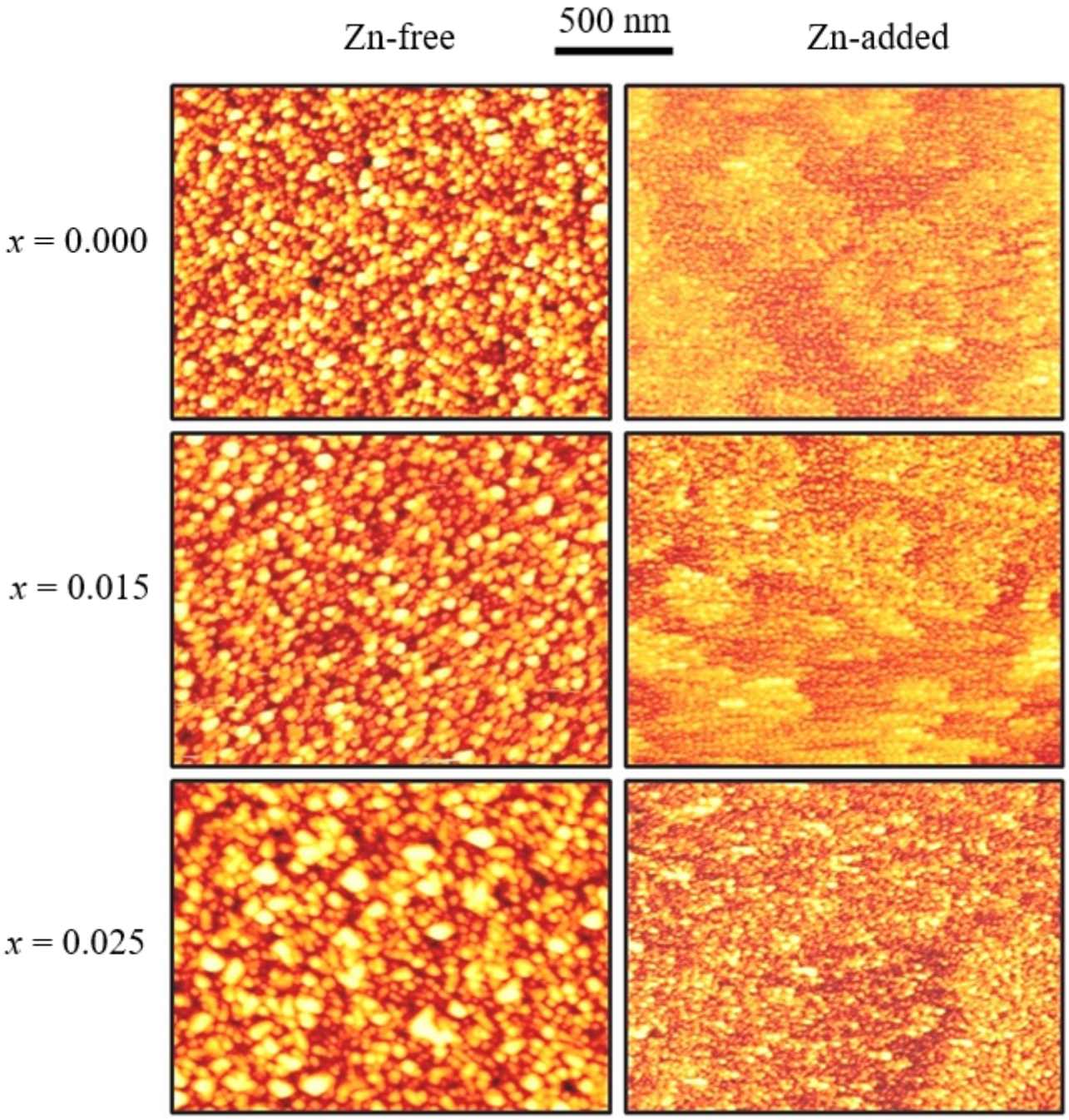


**Figure 1**

AFM images recorded from the surface of Zn-free and Zn-added as-grown films with x = 0.000, 0.015, and 0.025.

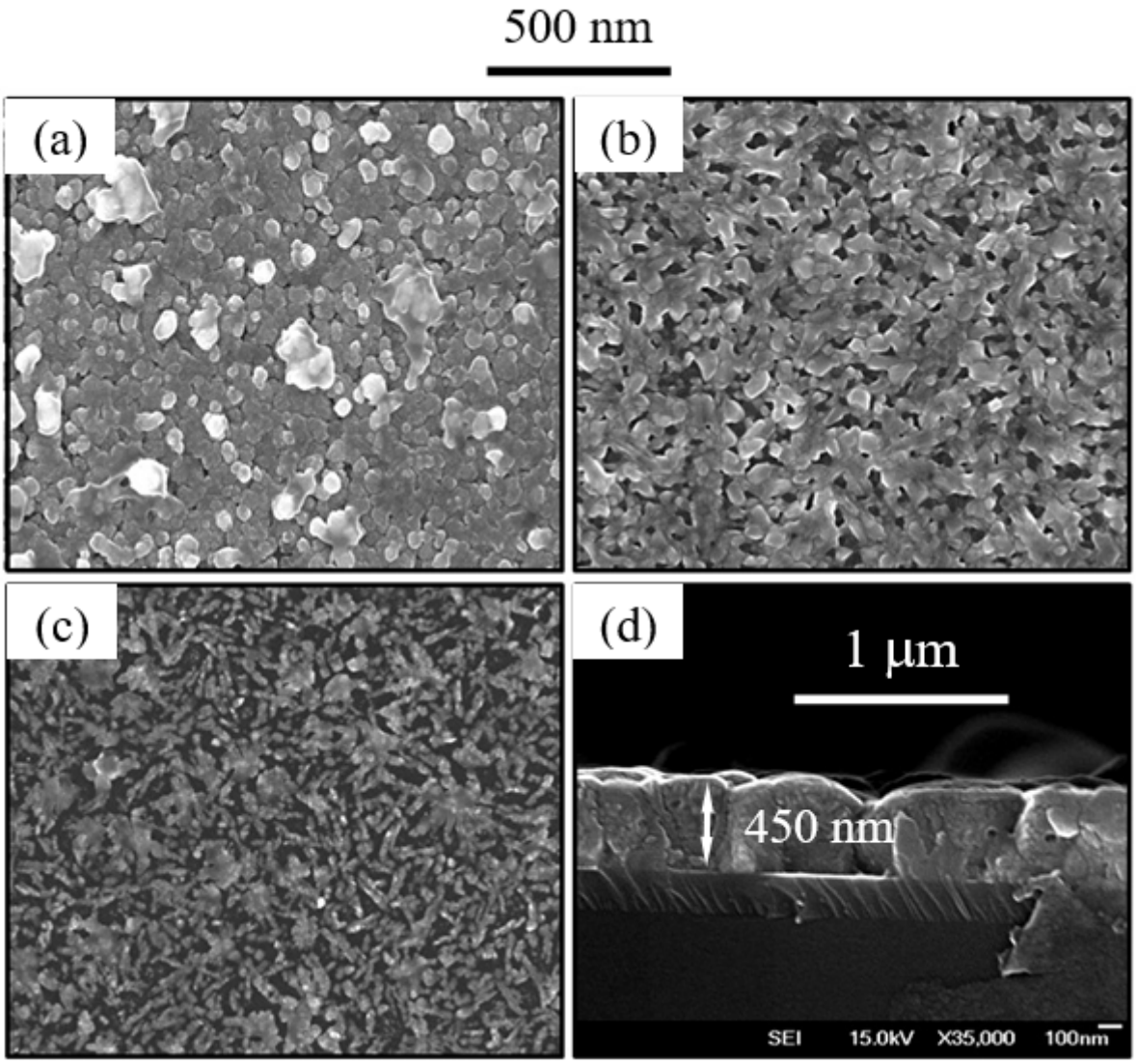


## Figure 2

FE–SEM images of the Zn-free as-grown films with high levels of Cu in solution: (a) x = 0.030, (b) 0.035, and (b) 0.040. (d) Cross-sectional FE–SEM image of the film with x = 0.020.

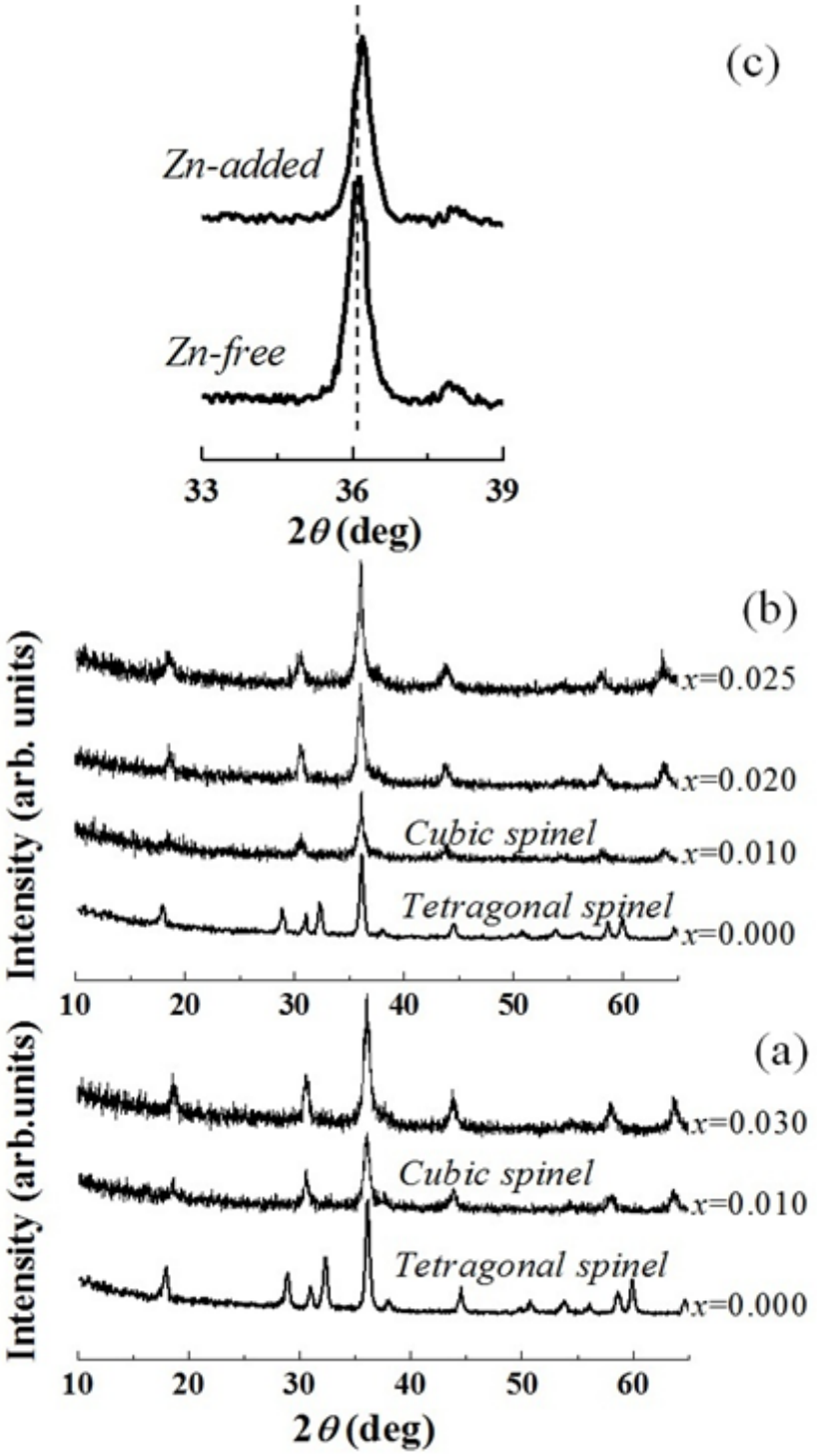


## Figure 3

XRD patterns of (a) Zn-free and (b) Zn-added films. (c) Enlarged tetragonal (221) peaks of Zn-free and Zn-added films at x = 0.000.

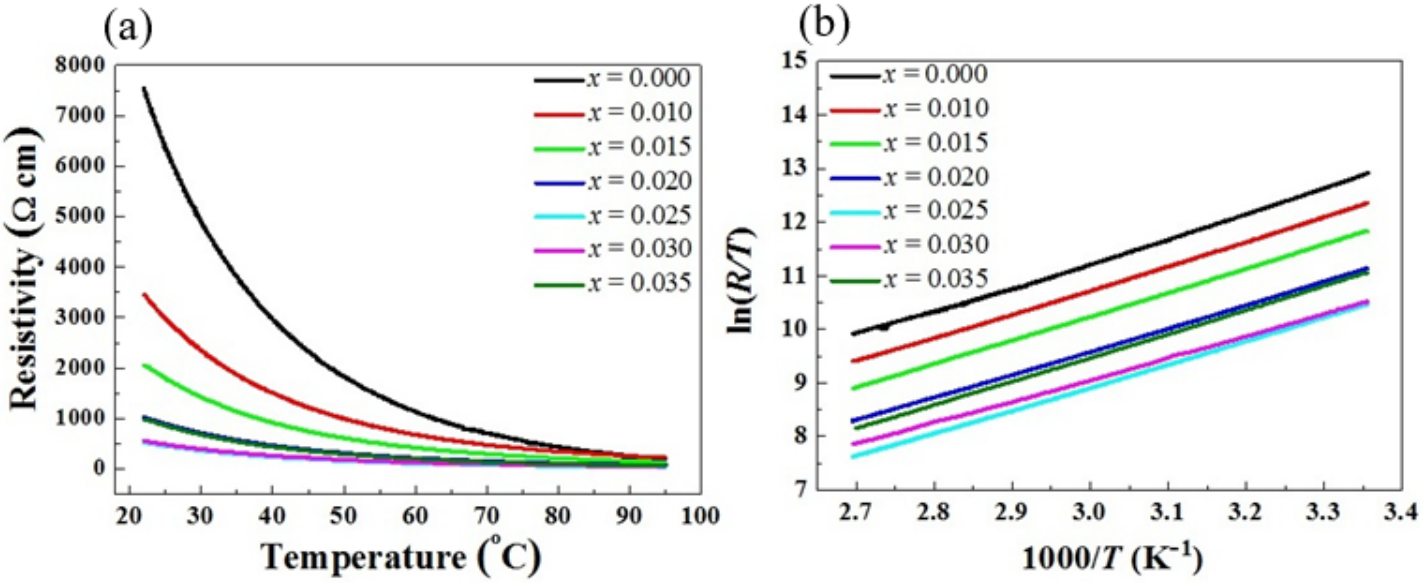


## Figure 4

(a) Resistivity–temperature (ρ–T) curve, (b) plot of ln(R/T) versus (1000/T) for the Zn-free films, examined as a function of x.

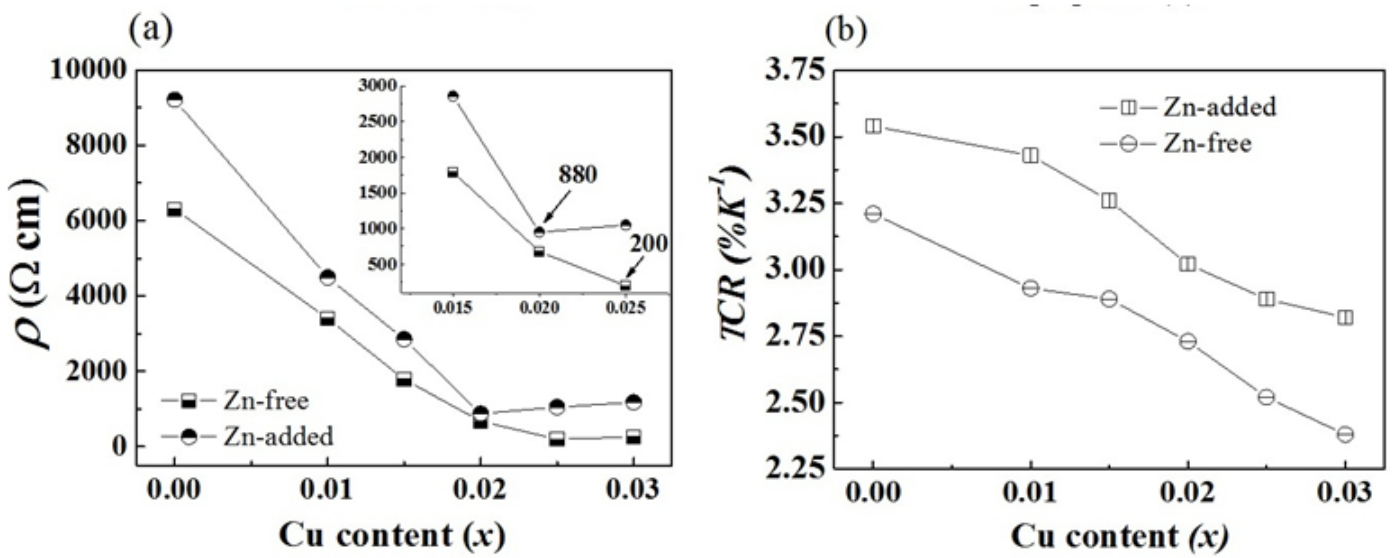


## Figure 5

Dependence on the Cu substitution level (x) of the (a) RT resistivity (ρ) and (b) absolute TCR of the Zn-free and Zn-added films. The inset in fig. 5a shows the lowest resistivity values attained for the Zn-free and Zn-added films within the investigated range of x.

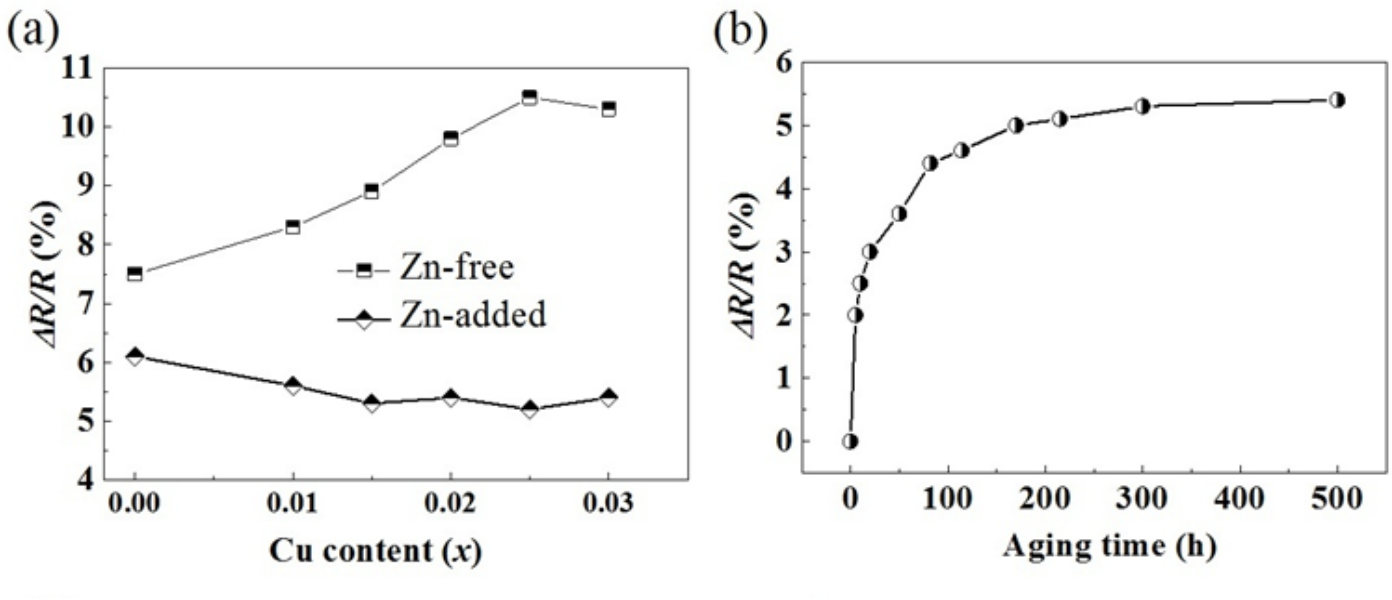


## Figure 6

(a) Resistance drifts of films with and without added Zn after 500 h of aging at 150 °C in air. (b) Resistance change history of the Zn-added film with x = 0.020.

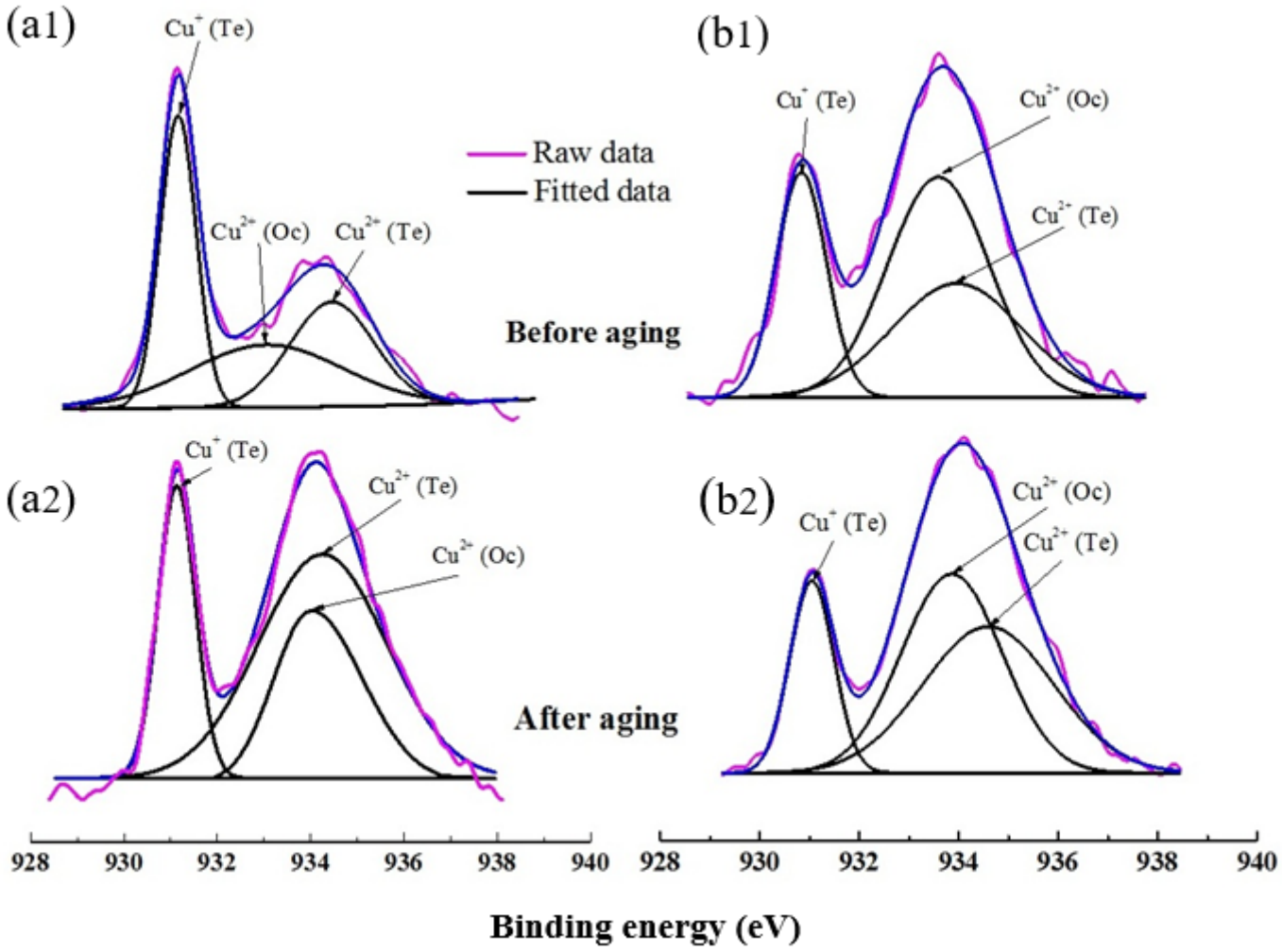


## Figure 7

(a) XPS spectra in the Cu2p3/2 core level of (a1–2) Zn-free sample with x = 0.025 and (b1–2) Zn-added sample with x = 0.020, examined before (top) and after (bottom) aging at 150 °C in air for 500 h.